nature sustainability

Article

https://doi.org/10.1038/s41893-023-01186-6

The spread and cost of saltwater intrusion in the US Mid-Atlantic

Received: 24 January 2023

Accepted: 28 June 2023

Published online: 20 July 2023

Check for updates

Pinki Mondal[1,2] ✉, Matthew Walter[1], Jarrod Miller[2], Rebecca Epanchin-Niell[3,4], Keryn Gedan[5], Vishruta Yawatkar[1], Elizabeth Nguyen[6] & Katherine L. Tully[6]

Saltwater intrusion on coastal farmlands can render productive land unsuitable for agricultural activities. While the visible extent of salt-impacted land provides a useful saltwater intrusion proxy, it is challenging to identify in early stages. Moreover, associated ecological and economic impacts are often underestimated as reduced crop yields in farmlands surrounding salt patches are difficult to quantify. Here we develop a high-resolution (1 m) dataset showing salt patches on farm fringes and quantify the extent of salt-impacted lands across the Delmarva Peninsula, United States. Our method is transferable to other regions across and beyond the mid-Atlantic with similar saltwater intrusion issues, such as Georgia and the Carolinas. Our results show that between 2011 and 2017, visible salt patches almost doubled and 8,096 ha of farmlands converted to marsh—another saltwater intrusion consequence. Field-based electrical conductivity measurements show elevated salinity values hundreds of metres from visible salt patches, indicating the broader extent of at-risk farmlands. More farmland areas were within 200 m of a visible salt patch in 2017 compared to 2011, a rise ranging between 68% in Delaware and 93% in Maryland. On the basis of assumed 100% profit loss in at-risk farmlands within a 200 m buffer around salt patches in 2016–2017, the range of economic losses was estimated between US$39.4 million and US$107.5 million annually, under 100% soy or corn counterfactuals, respectively.

With continued sea-level rise, coastal waters are reaching farther inland causing changes in soil salinity and water quality, leading to permanent land loss and ecosystem alterations[1–6]. In coastal counties of the United States, which hosts about 9% of all US farmlands[7], saltwater intrusion (SWI) into coastal ground- and surface-water results from a combination of natural sea-level variability and sea-level rise, land subsidence, drought and storm surges, the connectivity of the landscape to tidal channels and groundwater extraction[4,8–10]. Furthermore, SWI increasingly results from frequent far-reaching seasonal high tides, as opposed to solely from infrequent powerful storms, as was the more dominant driver a few decades ago[11]. With reported rates of sea-level rise twice the global average[9], the Mid-Atlantic region of the United States deserves special attention.

SWI is leading to a suite of ecological changes including increased soil salinity, visible salt patches on the soil, the formation of ghost forests and expansion of salt-tolerant invasive species[2,12]. Moreover,

[1]Department of Geography and Spatial Sciences, University of Delaware, Newark, DE, USA. [2]Department of Plant and Soil Sciences, University of Delaware, Newark, DE, USA. [3]Department of Agricultural and Resources Economics, University of Maryland, College Park, MD, USA. [4]Resources for the Future, Washington, DC, USA. [5]Department of Biological Sciences, George Washington University, Washington, DC, USA. [6]Department of Plant Science and Landscape Architecture, University of Maryland, College Park, MD, USA. ✉e-mail: mondalp@udel.edu

https://doi.org/10.1038/s41893-023-01186-6

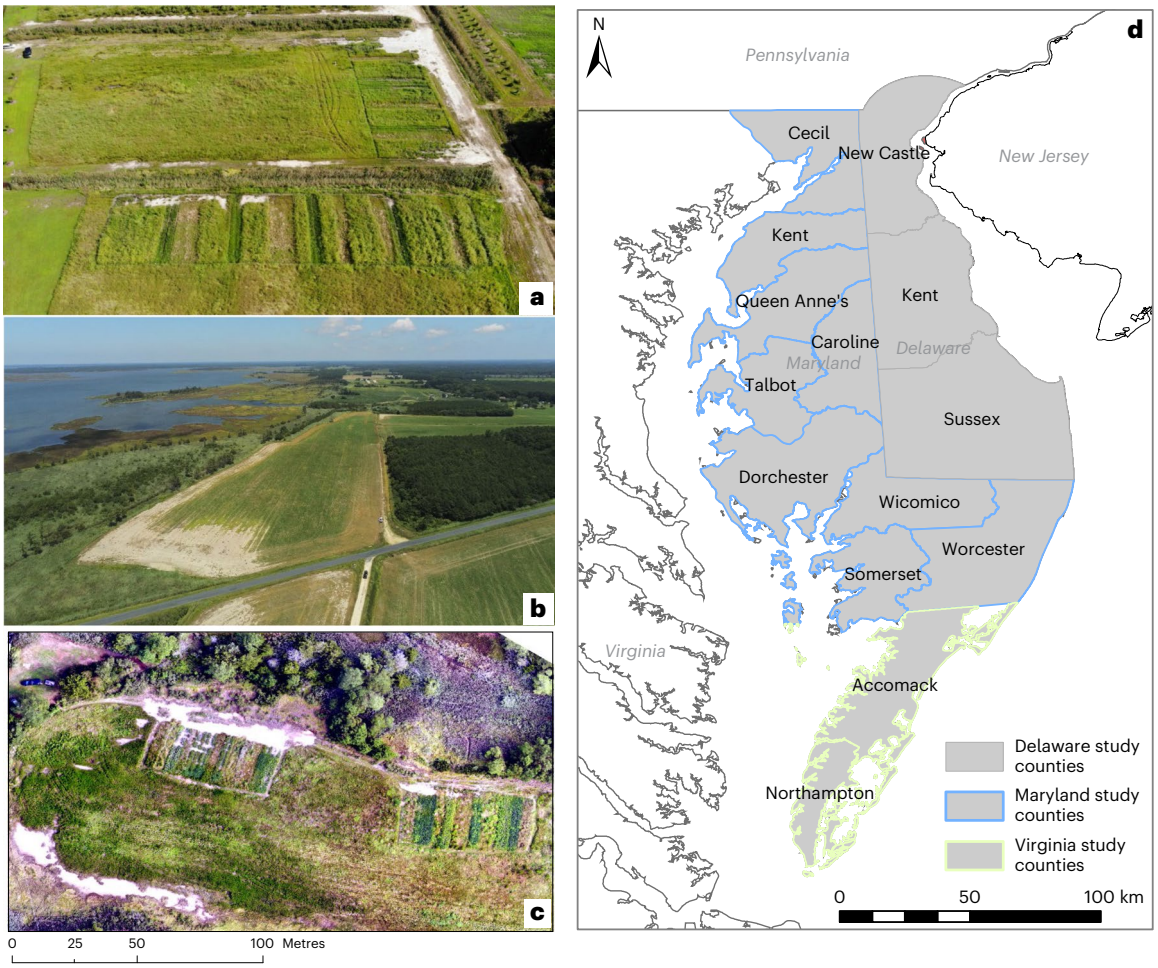

Fig. 1 | Where crops do not grow. a, Visible salt patches at the farm fringes. **b**, Many Delmarva farmlands are close to brackish or saline water. **c**, A drone image from a farm in Somerset County, Maryland (2019). **d**, Study area showing 14 coastal Delmarva counties in Delaware, Maryland and Virginia.

SWI can directly reduce crop yield, as most crops are highly sensitive to saline soil[13–16]. Yet, it is challenging to quantify agricultural losses due to SWI, since marginal yield losses are difficult to detect or quantify. Visible salt patches on farm fields, that typically occur near field edges, close to agricultural ditches and tidal creeks at the lowest lying points on the field (Fig. 1), can be used as a proxy for SWI mapping. However, documenting these salt signatures is challenging due to their fine spatial scale and patchiness, ranging from a few to hundreds of metres. Measuring the extent and severity of the impacts of SWI through field-based methods is labour-intensive, time-consuming and expensive. A more direct and cost-effective approach would be to use remotely sensed images (aerial and satellite data) and machine-learning approaches to identify white, reflective patches on the soil as salt signatures (Fig. 1). Combining field-based knowledge of salt patches in the study area and remote sensing techniques, we have developed a method that is efficient in identifying fine-scale salt patch features over a large geographic region.

We provide high-resolution mapping of visual evidence of salt patches on farmlands in the Delmarva Peninsula covering 1.54 million ha over 14 coastal counties in Delaware, Maryland and Virginia; an area that hosts 28.4% of the total harvested farmlands in those three states. At least 35% of the land on the Delmarva Peninsula is within 5 m of the high tideline[17]. Using a Random Forest (RF) algorithm trained and tested with 94,240 reference points, we mapped and quantified farmland in 14 counties that displayed transient or persistent salt patches between 2011 and 2017 (Fig. 2) and estimated the loss in profit from these salt-impacted farmlands. The 'salt patch' class in this study includes bright white salt patches along the farm fringes (Fig. 1), mostly found in elevation <1 m, as well as bright white patches scattered anywhere in a field. We further quantified the area that converted from salt patch, farmlands and bare soil into marsh (Fig. 3) that often represents the permanent loss in productive farmlands due to increasing soil salinity.

Our results show that the effect of salt patches on agricultural productivity extends far beyond what is currently mappable. For example, while the acreage of land with visible salt patches may be small, its presence denotes that the entire field is at risk of conversion to saline soil unsuitable for traditional farming. Further, in some instances, soil salinity in nearby areas of the field may be high enough to reduce crop yield but not enough to leave bare patches. To identify farmlands at the greatest risk of SWI, we calculated the acreage of corn and soybeans within 50, 100 and 200 m buffers around the existing salt patches using the United States Department of Agriculture (USDA) Cropland Data Layer[18]. We selected these distances on the basis of measurements of soil electrical conductivity (EC) collected from 36 farm sites (Supplementary Fig. 1; Methods). Our choice of corn and soybeans as preferred crops is because the Delmarva economy is dominated by corn–soybean farming.

Most farmlands on the Delmarva Peninsula are planted in grain crop rotations during summer (for example, corn–soybean). While soybean is more tolerant to salt[13], corn is a more profitable crop. Due to the ongoing and increasing SWI effects, crop yields in affected sites are expected to decline over the coming years[15,19,20]. In an attempt to quantify the range in potential losses in profit from increased soil

https://doi.org/10.1038/s41893-023-01186-6

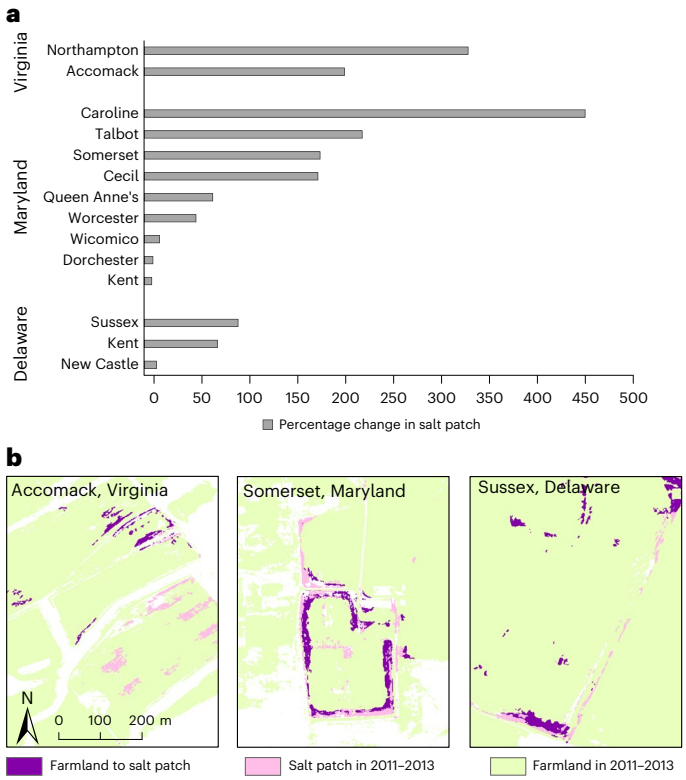

Fig. 2 | Changes in visible salt patches between 2011–2013 and 2016–2017. **a**, Percentage change in total area of visible salt patches. **b**, Regions in the study area highlighting farmlands that converted to salt patches between 2011 and 2017 (in purple).

salinization, we used an 'enterprise budget' (Methods) that considers yields, land rental, fertilizer prices and harvested grain prices for three scenarios: (1) 'business-as-usual' where the at-risk farmlands have the current corn and soybean acreage, (2) 'corn counterfactual' (assuming at-risk farmlands with corn and soybean combined have 100% corn, thus 100% annual profit from corn) and (3) 'soybean counterfactual' (assuming at-risk farmlands with corn and soybean combined have 100% soybean, thus 100% annual profit from soybean). We estimated potential losses assuming zero profits (not zero yield) on salt patches and surrounding farmland within 50, 100 and 200 m buffers, relative to a counterfactual of average profits under high yields. In addition, we estimated potential losses assuming a reduced 80% yield for the two counterfactual scenarios. Counterfactual profits (potential losses) were calculated on the basis of average 10 year input, crop prices and the highest reported annual county-based crop yields[21].

Results

Visible salt patches expanding at an alarmingly high rate

Salt patches, associated with very little to no plant growth, represent a complete loss of productive land. About 472 ha of land across the Delmarva Peninsula, mostly near field edges, had visible salt patches during 2011–2013 (Fig. 2). This area nearly doubled to 905 ha during 2016–2017 and varied greatly by county. The nine coastal Maryland counties experienced a 79% increase in salt patch area. In Delaware and the Eastern Shore of Virginia, the area of salt patches increased 81% and 243%, respectively, between 2011 and 2017. While the expansion rate is alarming, the absolute area of these identified salt patches remained small in 2017: about 445 ha in Maryland; 339 ha in Delaware; and 122 ha in Virginia. The rate of change between time-steps varied across the counties with numbers ranging from a 7.6% increase in Kent County to a 450.5% increase in Caroline County, both in Maryland (Fig. 2). Salt patches remained a small fraction of total land cover across Delmarva, ranging between 0.01% and 0.18% of total farmlands in a given county in 2011–2013 and between 0.01% and 0.39% in 2016–2017 (Fig. 4a). Moreover, appearance and disappearance of salt patches varied over time, with only 24 ha of visible salt patches identified in the period 2011–2013 remaining visible in 2016–2017 (8.7 ha in Maryland, 15 ha in Delaware and 0.6 ha in Virginia). The overall expansion of salt patches was largely due to 436, 323 and 121 ha of new salt patches that appeared in 2016–2017 in Maryland, Delaware and Virginia, respectively. About 36% and 32% of the salt patch area are located on sites with elevation <2 m during 2011–2013 and 2016–2017, respectively.

Farmlands at risk from further saltwater intrusion

Increasing soil salinity might result in gradual conversion of farmlands to marsh[22]. We estimated that about 36.5 ha of land was converted from salt patch to marsh and about 1,007 ha of land was converted from bare soil to marsh between 2011 and 2017 across our study area. Over 188 ha and 275 ha of bare soil converted to marsh between 2011 and 2017 within the 100 and 200 m buffers, respectively. In addition, over 8,096 ha of farmland was converted to marsh across the 14 coastal Delmarva counties between 2011 and 2017 (Fig. 3). The three Delaware counties have the largest share of such conversions at 3,824 ha, followed by the nine counties in Maryland (3,488 ha) and two counties in Virginia (784 ha). These converted lands are more suitable for salt-tolerant species[14,16,23], including both native marsh species and salt-tolerant invasive species such as the common reed (the Eurasian lineage of *Phragmites australis*).

We estimated about 13,732 ha of at-risk farmland across the Delmarva Peninsula during 2011–2013 that are located within 50 m of a visible salt patch. By 2016–2017, that number grew to about 28,022 ha or about three-quarters the size of Philadelphia. The increase in at-risk farmlands varied by state—from 4,726 to 9,150 ha in the three Delaware counties (94% increase), from 1,321 to 2,636 ha in the two Virginia counties (99% increase) and from 7,684 to 16,236 ha in the nine Maryland counties (111% increase). Between the two time-steps, this represents a change from 2.5% to 5.2%, 2.3% to 4.3% and 1.9% to 4.1% of total farmlands in the study counties in Virginia, Delaware and Maryland, respectively. In 2011–2013, these at-risk farmlands represented between as little as 0.4% of all farmlands in Cecil County, Maryland, to up to 4.7% of all farmlands in Somerset County, Maryland (Fig. 4b). In 2016–2017, the range of at-risk farmlands increased to a minimum of 1.6% in Kent, Maryland, and a maximum of 8% in Somerset, Maryland (Fig. 4b).

We found that ~35,032 ha of farmland were within 100 m of a salt patch during 2011–2013, which increased to 68,475 ha, or about twice the size of Philadelphia, during 2016–2017. Delaware counties experienced a rise in at-risk farmlands from 12,368 to 22,416 ha (81%), whereas the counties in Virginia and Maryland had an increase from 3,250 to 6,283 ha (93%) and from 19,414 to 39,775 ha (105%), respectively. This represents an increase from 6% to 12.2%, 6% to 10.5% and 4.7% to 10.1% of the total farmlands in the study counties in Virginia, Delaware and Maryland, respectively. The distribution pattern remains the same as was seen for at-risk farmlands within a 50 m buffer. Somerset County, Maryland, had the largest share for both time-steps (11.7% and 16.9%; Fig. 4c).

Using a more liberal estimate of the area around visible salt patches in which crop yields may be affected, we found that about 91,073 and 166,930 ha of at-risk farmland was within 200 m of a visible salt patch during 2011–2013 and 2016–2017, respectively. The study counties in Delaware, Virginia and Maryland witnessed a rise in at-risk farmlands from 33,064 to 55,511 ha (68%), 8,095 to 14,898 ha (84%) and 49,914 to 96,521 ha (93%), respectively (Fig. 4d). This represents an increase from 16.1% to 26.1%, 15% to 29.4% and 12.2% to 24.5% in the study counties in Delaware, Virginia and Maryland, respectively. It is noteworthy that crop stress due to soil salinization does not decline linearly with distance from a visible salt patch. In other words, the deleterious effects experienced by crops do not depend on their exact location within

https://doi.org/10.1038/s41893-023-01186-6

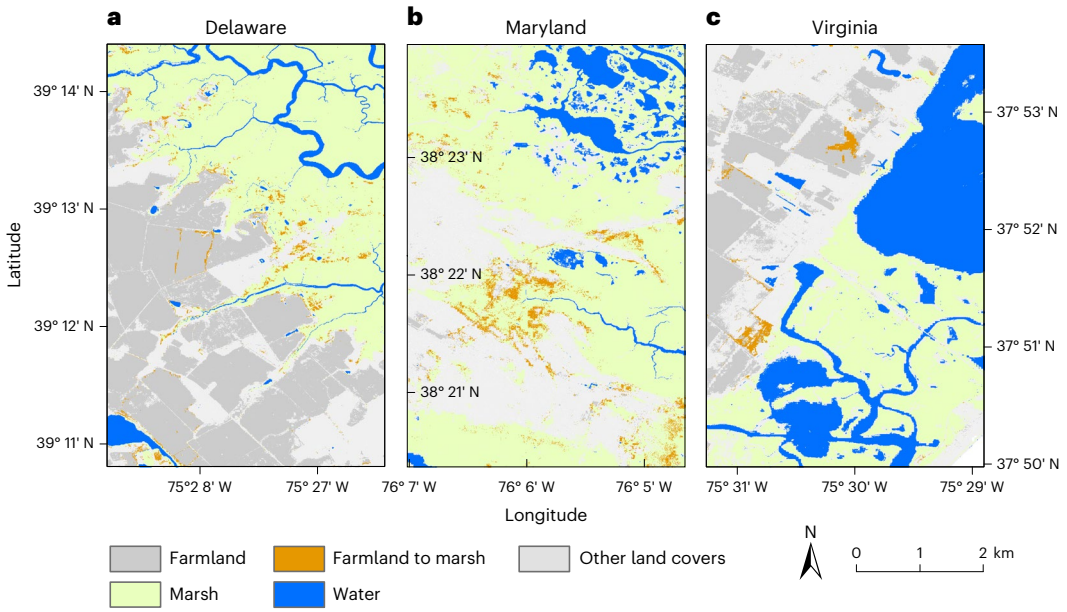

Fig. 3 | Conversion of farmlands to marsh between 2011–2013 and 2016–2017. a–c, Changing landscapes in Kent, Delaware (**a**); Dorchester, Maryland (**b**); and Accomack, Virginia (**c**).

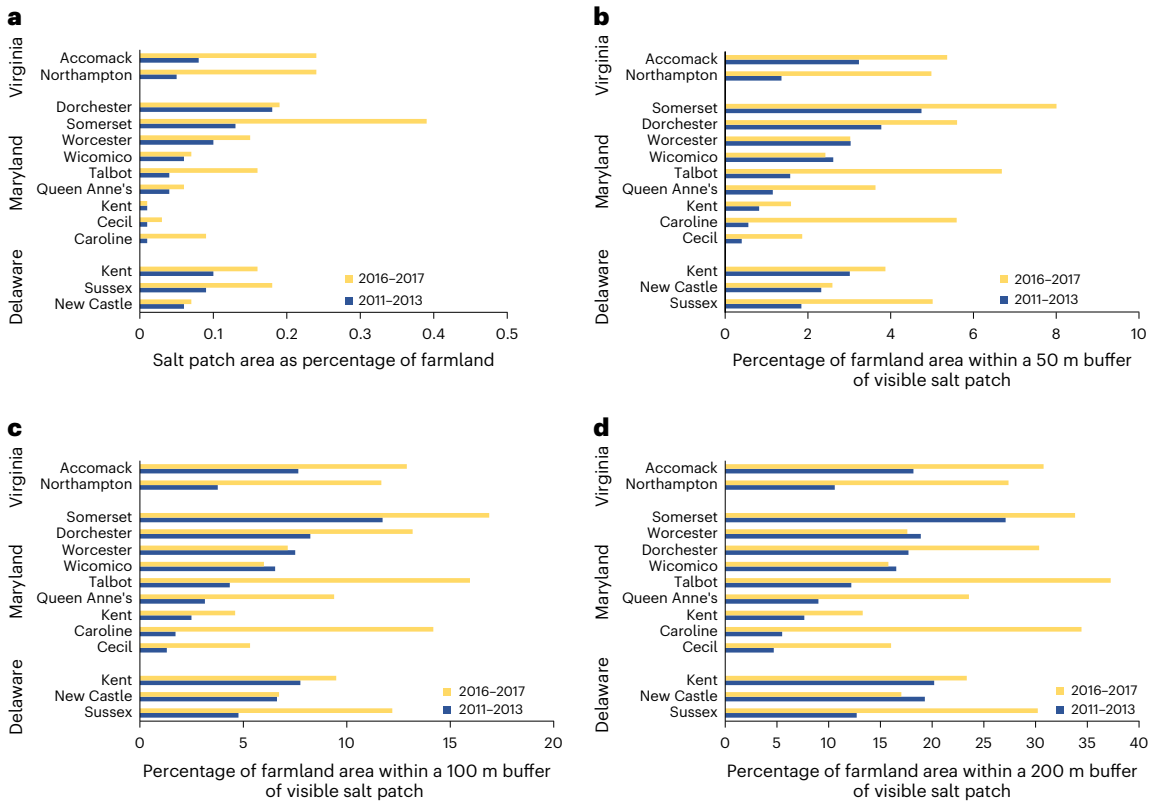

Fig. 4 | Changes in salt patches and at-risk farmland around these patches between 2011–2013 and 2016–2017. a, Change in salt patch area as a percentage of farmland for each county. **b–d**, Change in the extent of at-risk farmlands within 50 m (**b**), 100 m (**c**) and 200 m (**d**) of salt patches for each county.

these buffers per se, as we recorded similar soil EC values in all these buffers (Supplementary Fig. 1).

Substantial profit loss from saltwater intrusion on Delmarva

Within the buffers around the salt patches, the sources of financial losses stem from both observed salt patches and potential salinization of the adjacent farmlands, thereby reducing yield and profit. It is not possible to estimate the exact percentage of loss in profit due to the varied levels of salinity in farmlands where salt patches are not visible yet. Hence, we first estimated an upper bound in these losses with the assumption of zero profit on the salt-impacted farmlands, both salt patches and farmlands within these buffers, planted in corn or soybean. Loss estimates are based on the assumption that yields on salt-affected lands generate revenue that only just covers input costs, as

opposed to assuming zero yields, which would induce financial losses if crops were planted. We calculated foregone profits (potential losses) on the basis of high yield and average per bushel profits over 10 years (2011–2020) in each county (Fig. 5). Then we estimated subscenarios within our two counterfactuals (100% profit coming from corn and soybeans, respectively) assuming a 20% yield loss, that is 80% crop yield potential. It should be noted that the same level of salinity would result in different yield decline for corn and soybeans.

Business-as-usual scenario. Considering the current scenario in which profits are derived from corn and soybeans, planted in rotation, we estimated an annual loss in profit from visible salt patches ranging between US$101,642 (considering 2011–2013 salt patches) and US$325,419 (considering 2016–2017 salt patches) (Fig. 5a). Since corn is more profitable, the higher share of loss also comes from corn—US$67,202 for 2011–2013 and US$234,017 for 2016–2017. These 'loss in profit' values from corn consist of about 66–72% of the total loss in profit. Sussex County in Delaware showed the most increase in potential losses, estimated at US$84,431 (Fig. 5a).

Considering all farmlands within 50 m buffers around the salt patches, we estimated the losses in profit to be US$5.8 million in 2011–2013 and US$11.9 million in 2016–2017 (Fig. 5d). For 100 m buffers, our estimated annual profit loss ranged between US$14.9 million in 2011–2013 and US$29 million in 2016–2017 (Fig. 5g). For 200 m buffers, the estimated annual profit loss ranged between US$39.3 million in 2011–2013 and US$70.7 million in 2016–2017 (Fig. 5j). Out of this total loss in profit, the share of corn is 70–71% for all three buffer estimates. Delaware's Sussex County had the most losses in profit under a business-as-usual scenario, estimated at US$3.1 million (50 m buffer), US$7.4 million (100 m buffer) and US$18.5 million (200 m buffer) in 2016–2017.

Corn counterfactual scenario. Focusing only on visible salt patches and assuming zero profits in these locations over a 10 year average, we estimated potential annual losses of US$163,963 across the Peninsula in 2011–2013 (Fig. 5b). By 2016–2017, the potential financial losses tripled to US$493,138, owing to the increase in the extent of salt patches. We estimated the highest profit loss in Sussex County in Delaware at US$160,000 in 2016–2017, also showing the largest increase in losses between the two time-steps (Fig. 5b).

Extending our analysis to the 50 m buffer on at-risk farmlands adjacent to visible salt patches, we estimated a potential profit loss in the range US$8.7 million (2011–2013) to US$18.1 million (2016–2017) under a 100% corn scenario (Fig. 5e). Considering a 100 m buffer around each observed salt patch (Fig. 5h), the potential losses for the Delmarva Peninsula ranged between US$22.2 million (2011–2013) and US$44.1 million (2016–2017). Considering a 200 m buffer (Fig. 5k), the potential losses in profit ranged between US$58.3 million (2011–2013) and US$107.5 million (2016–2017). The top three counties from each state with the largest share of losses are Sussex (Delaware), Dorchester (Maryland) and Accomack (Virginia) for all buffers in 2016–2017 (Fig. 5).

Within this 100% corn counterfactual, we further considered a 20% yield loss scenario and estimated a profit loss range of US$4.8 million (2011–2013) to US$10.1 million (2016–2017) in the 50 m buffer. Considering the 100 m buffer, the profit loss ranged between US$12.3 million (2011–2013) and US$24.7 million (2016–2017). For the 200 m buffer, the assumed yield loss resulted in an estimated profit loss ranging between US$32.5 million (2011–2013) and US$60.5 million (2016–2017).

Soybean counterfactual scenario. Since soybeans are less profitable than corn, a counterfactual scenario with 100% soybean generates the least potential losses due to SWI. For this counterfactual, we estimated potential losses of US$59,186 from visible salt patches across the Peninsula in 2011–2013, almost half of the estimated losses in the business-as-usual scenario (Fig. 5c). For 2016–2017, the potential losses in this counterfactual tripled to US$178,746 but were still only about one-third of the potential losses in a 100% corn counterfactual scenario.

For 50 m buffers (Fig. 5f), estimated losses in profit across the Peninsula ranged between US$3.2 million (2011–2013) and US$6.6 million (2016–2017). For 100 m buffers (Fig. 5i), our estimated losses in profit ranged between US$8.4 million (2011–2013) and US$16.1 million (2016–2017). Considering a 200 m buffer (Fig. 5l), the potential losses in profit ranged between US$22.2 million (2011–2013) and US$39.4 million (2016–2017). The potential losses for this counterfactual were the largest for Sussex County in Delaware, estimated at US$1.5 million (50 m buffer), US$3.6 million (100 m buffer) and US$8.9 million (200 m buffer) in 2016–2017 (Fig. 5).

In a 20% yield loss scenario under a 100% soybeans counterfactual, we estimated a profit loss of US$2.6 million (2011–2013) to US$5.4 million (2016–2017) in the 50 m buffer. The losses in profit increased to US$6.6 million (2011–2013) and US$13.2 million (2016–2017) in the 100 m buffer. With the same yield loss assumption, we estimated a range of profit loss between US$17.5 million (2011–2013) and US$32.4 million (2016–2017) in the 200 m buffer.

Discussion

The mid-Atlantic region of the United States has been witnessing rapid landscape-level changes over the last few decades[6,24,25]. This study documents visible salt patches and their spatiotemporal evolution across the Delmarva Peninsula. Our results show that the rapid growth of salt patch area across the Delmarva during the last decade is notable. Bare areas in farm fields displaying the distinct signature of SWI nearly doubled (92% increase) during the 6 years of the study period (2011–2017), as did the potential losses in profit in at-risk farmlands.

While visible salt patches are a good indicator of the spatial distribution of salt-impacted farmlands, their absence may not necessarily indicate a productive farmland or absence of SWI; high salinity areas may not be equally visible at all times. Various factors ranging from farming practices to regional climate and weather events may modify identifiable salt patches on the ground. For example, following a large rain event, farm abandonment or a fallow period[26,27], salt patches may not be visible in aerial images. Compared to drier climates, the Delmarva Peninsula receives an average rainfall of 1,140 mm rainfall annually[28]. This is usually enough to dilute and remove salts from the soil surface and to allow plants to germinate[16]; yet, the water table in our study region is often close enough to the surface that the saline water has nowhere else to go. Moreover, soil salinity may increase incidentally following nuisance flooding[29] or weather events such as northeasters or hurricanes, which push salts inland and may increase the visibility of salt signatures in remotely sensed data. The addition of salts at later crop growth stages may reduce yields[30], without causing bare patches. As such, visible salt patches and the approach of estimating at-risk farmlands using buffers around them should be considered a highly conservative estimate of farmlands affected by SWI.

On the basis of our findings, it is a reasonable assumption that all visible salt patches indicate land presently affected by SWI or the very frontlines of coastal changes due to sea-level rise. Visible salt patches are ephemeral, often occurring before farm abandonment and land use change. However, widespread marsh conversion in the study region denotes a strong directional change in land covers as a SWI consequence. About 36.5 ha of salt patch area converted to marsh, while 8,096 ha of farmland in the Delmarva Peninsula converted to marsh during the 6 year study period, which exceeds the area of fields exhibiting salt patches and suggests that sea-level rise is a substantial source of land cover change in this region. Moreover, the extent of sea-level rise impacts appears to be growing; we estimated that in 2016–2017 between 28,022 (using a 50 m buffer) and 166,930 (using a 200 m buffer) additional hectares of farmland were at-risk on the Peninsula due to their proximity to the visible salt patches. Evidently, the effects of sea-level rise and SWI are far more extensive than what is visible at the surface.

https://doi.org/10.1038/s41893-023-01186-6

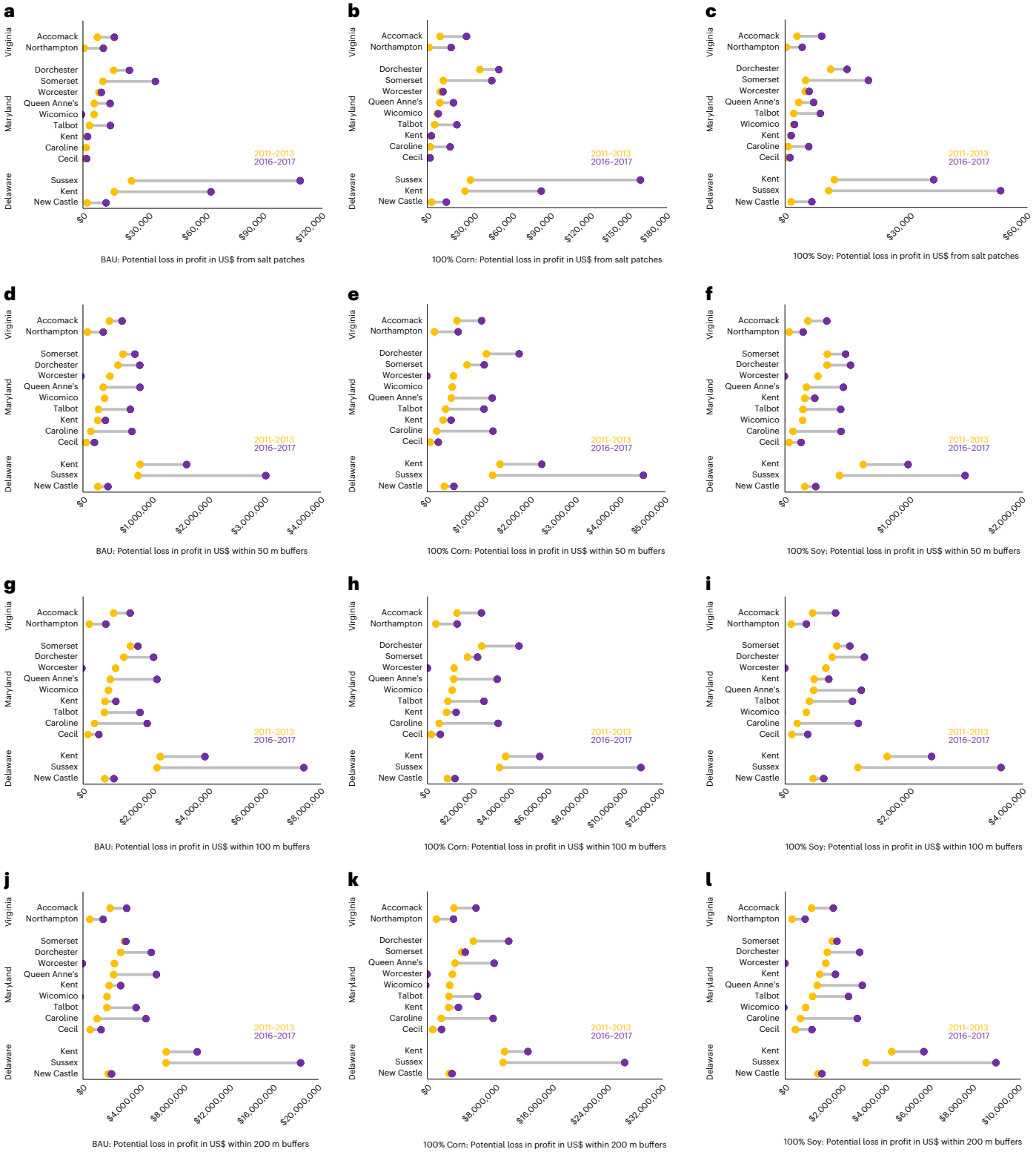

Fig. 5 | Potential loss in profit in US$ from salt patches and at-risk farmlands considering 10 year averages in crop prices. a–**c**, Potential losses from salt-affected lands. **d**–**f**, Potential losses in salt-adjacent lands within a 50 m buffer. **g**–**i**, Potential losses in salt-adjacent lands within a 100 m buffer. **j**–**l**, Potential losses in salt-adjacent lands within a 200 m buffer. Each panel row shows three scenarios: business-as-usual (BAU) where profit is derived from both corn and soybean (**a**,**d**,**g**,**j**), a corn counterfactual where 100% profit comes from corn (**b**,**e**,**h**,**k**) and a soybean counterfactual where 100% profit comes from soybean (**c**,**f**,**i**,**l**). Yellow and purple circles represent profit losses using salt patch estimates from 2011–2013 and 2016–2017, respectively, whereas the grey bars denote the change in estimated losses in profit.

These changes are of great economic concern and having a visible signal of contemporary sea-level rise presents an opportunity to detect the geographic distribution of sea-level impacts in near real-time, which holds promise for a number of future applications. From a basic science perspective, real-time tracking will enable greater mechanistic understanding and improved ability to model SWI. For example,

empirical models based on spatial correlations could help us to better understand the role of ditch and canal networks[31], soil characteristics and geologic features[32], legacies of land reclamation[33,34] or water table levels and recharge[35–37]. Greater understanding of how human activities exacerbate or reduce salt patches and marsh, such as the construction or removal of tide gates and berms, should be of particular interest to policy-makers. Real-time tracking could also be used to better understand the distribution and inequity of economic impacts in the coastal zone, knowledge of which could be used to design and target new incentive programmes to the landowners who most need them in the changing coastal landscape. Our high-resolution geospatial datasets provide a finer spatial resolution compared to global datasets, such as the Global Map of Salt-affected Soils or GSASmap[38]. This level of detail is critical for the farm-level decision-making that is often required to design and implement state-level policies.

Our work provides evidence for an immediate policy attention required to protect the coastal lands against increasing soil salinization. Due to its sensitivity to salinity, the corn-focused agricultural economy is not suitable for many SWI-affected coastal fields across Delmarva. Increasing the share of farmlands under more salt-tolerant crops (for example, soybeans, sorghum or barley), reducing inputs, adding gypsum to the salt-affected lands or using crop insurance as a strategy to limit losses and delay transitions might result in lower economic losses in the immediate future. However, landowners might be forced to abandon these farmlands once the soil becomes salinized beyond the tolerance of any traditionally farmed food crops. Recent studies have examined alternative crops, such as barley, quinoa and sorghum that might be more suitable for these landscapes[16]. Other adaptation strategies might include a controlled conversion of these landscapes into marsh that can support wildlife or act as a barrier to encroaching seawater[39]. While such transitions are vital to sustainable solutions, the fate of such coastal frontier zones will be shaped by the salinity gradient across these evolving landscapes. In highly salinized regions, halophytes might contribute to further soil salinization through continued and efficient water uptake in brackish soils—an example of a positive feedback loop[40,41]. Conversely, marsh vegetation might protect comparatively less salinized regions from further salt accumulation[42].

SWI is rampant across the North American Coastal Plain, from Massachusetts, United States, in the north to Northern Mexico in the south, with documented coastal forest loss[6]. This study highlights another SWI consequence that has far-reaching implications for the US economy as well as coastal ecosystems, by drawing attention to the gradual loss of productive Delmarva farmlands from SWI. Due to the reliance on freely available aerial and satellite images and well-established machine-learning methods, our geospatial method is transferable to other coastal regions across and beyond the mid-Atlantic with known SWI issues[1]. While other long-term SWI consequences, such as the expansion of ghost forests along the US coasts, have been documented in recent studies[1,6], the elusive nature of salt patches posed a challenge in estimating agricultural losses. Our high-resolution datasets not only address that challenge but also provide a baseline and a reproducible approach that can be used to track the spread and cost of SWI in the Delmarva Peninsula and beyond.

Methods

Aerial and satellite imagery

To quantify land uses/covers, including salt patches, across the Delmarva Peninsula we used aerial imagery from the National Agriculture Imagery Program (NAIP). NAIP images are high-resolution (1 m) aerial images containing red, green, blue and near-infrared (NIR) bands that are collected by the USDA on an ~3 year basis. We accessed orthorectified NAIP images from June–July 2011 (Maryland), May 2012 (Virginia), September 2013 (Delaware), June 2016 (Virginia), June 2017 (Maryland) and July–August 2017 (Delaware) on the Google Earth Engine (GEE) platform and developed high-resolution datasets for the study area for two time-steps: 2011–2013 and 2016–2017. In addition to the visible (red, green and blue) and NIR NAIP spectral bands, we calculated several other bands to be used as the inputs to the machine-learning based classification scheme. The additional bands include (1) four principal component analysis (PCA) bands derived from the four original NAIP bands using eigen analysis, (2) one normalized difference vegetation index (NDVI) band ((NIR − Red)/(NIR + Red)), (3) one normalized difference water index band ((Green − NIR)/(Green + NIR)), (4) one shadow index band ((256 − Blue) × (256 + Blue)) and (5) four smoothed bands derived from the four original NAIP spectral bands smoothed with a 3 × 3 boxcar kernel[43–45]. Each input band has a spatial resolution of 1 m. The derived bands are used to overcome unique challenges associated with high-resolution NAIP images used as inputs for land cover classifications, such as low spectral resolution, shadows and limited acquisition dates[46]. For example, PCA is a data reduction technique that converts correlated variables into a new set of uncorrelated variables and in remote sensing can be used to remove redundant information and enhance the details[47,48]. We followed the eigen analysis workflow in GEE to create four additional PCA bands by converting the four original NAIP bands into a one-dimensional array, calculating a covariance matrix, calculating eigenvalues and eigenvectors, using eigenvectors to transform the original array and finally normalizing the components[49]. In addition, shadows from tree crowns are a persistent problem and were addressed using the shadow index; NDVI and normalized difference water index aided in differentiating marsh and wetland vegetation from other green vegetation; and the smoothed bands reduced the speckle effect created by the high-resolution dataset.

NAIP-based classification, however, could only achieve an accuracy up to 75%, primarily due to the challenges stemming from its very high spatial resolution and the lack of seasonal information since all NAIP images are from summer/early autumn. We used moderate-resolution satellite images from Landsat to overcome these challenges and incorporate additional spectral information. Landsat is a series of satellites launched by the National Aeronautics and Space Administration with satellite images distributed through the United States Geological Survey. Landsat data include red, green, blue, NIR, shortwave infrared, aerosol, cirrus, panchromatic and thermal bands. All bands are collected at a 30 m resolution except the panchromatic band, which is collected at a 15 m resolution and the thermal bands which are collected at a 100 m resolution. Cloud-masked top-of-atmosphere (TOA) reflectance images from Landsat 5 (2011 and 2012), Landsat 7 (2013) and Landsat 8 (2016 and 2017) were obtained using GEE. To capture seasonal changes in vegetation, we derived four seasonal enhanced vegetation index (EVI) bands from the TOA images using this formula: 2.5 × ((NIR − Red)/(NIR + 6 × Red − 7.5 × Blue + 1)) (ref. 50). The coefficients used in the EVI equation are sensor-specific, hence we could not use EVI for NAIP images. We initially used NDVI for both NAIP and Landsat; however, for Landsat, EVI was preferred over NDVI because it yielded a higher accuracy. Each of the four EVI bands is a median of a different season: summer (June–August), autumn (September–November), winter (December–February) and spring (March–May). The EVI bands were smoothed with a 3 × 3 boxcar kernel to reduce noise[51]. These four EVI bands capture seasonal differences across spring, summer, autumn and winter. Thermal bands from the TOA images were also used to capture differences between non-vegetated surfaces such as sand, bare soil and buildings. Landsat 5 contains one thermal band (B6) while Landsat 7 and Landsat 8 contain two bands (B10 and B11). Again, a median was calculated to create a band for each of the four seasons and the bands were smoothed using a 3 × 3 boxcar kernel.

Random Forest classifier

A supervised classification using the RF algorithm was used to classify land uses/covers across the Delmarva Peninsula[52]. The input data used for the RF are comprised of the four NAIP bands, four PCA bands from NAIP, three indices from NAIP, four smoothed NAIP bands, four

smoothed seasonal EVI bands from Landsat and four (from Landsat 5) or eight (from Landsat 7 and 8) smoothed seasonal thermal bands. Landsat images were overlaid on NAIP images, so that the pixel values from different Landsat bands can be assigned to all the NAIP pixels residing within that particular Landsat pixel. This step ensured providing more spectral information to the RF classifier required to differentiate between spectrally similar land cover classes, such as farmland and residential neighbourhood lawn. The data used to test and train the RF were a combination of coordinates from ground data collected during summer of 2019 and reference points collected by visually assessing the NAIP imagery. In total, 94,240 points were collected spanning over both time-steps (Supplementary Table 1). We split these reference data using 70% of the points to train the RF and 30% to test the accuracy of the classification. The RF algorithm separates the data into eight defined land use/cover classes: forest, marsh, salt patch, built, open water, farmland, bare soil and other vegetation. We used the GEE platform for running the RF algorithm from the statistical machine intelligence and learning engine. The hyperparameters were set to 100 for the number of trees and the default values for variables per split (4), minimum leaf population (1), bag fraction (0.5) and max nodes (no limit). We ran a separate RF classifier for each state–year combination to avoid confusing the classifiers with a range of values for the same land cover across space and time. This is a widely used method for postclassification change detection.

Postprocessing

Due to the high resolution of the input data, there is a considerable 'salt-and-pepper effect' or speckle effect on the classified image. Such effects are more visible in the salt patch class and its surroundings compared to other land covers (due to larger sample size, that is number of pixels). As a postprocessing step to reduce such speckle effects, we applied a majority filter to the classified image using the Focal Statistics tool in ArcGIS Pro v.3.0.3 with a 3 × 3 pixel neighbourhood. For example, any solitary salt patch pixel was 'reclassified' as the majority land cover within the immediate neighbourhood. Furthermore, we considered only patches of ten or more connected 'salt patch' pixels as a valid salt patch. We also used a road mask to minimize the confusion between impervious streets and salt patches. Figures were created using ArcMap 10.8.1 and Microsoft PowerPoint 2016.

Accuracy assessment

To determine the accuracy of the classification, we compared about 30% of points (n = 30,414) withheld from the RF algorithm to the classified image results. From the resulting confusion matrix, we calculated several accuracy estimates: user's accuracy, producer's accuracy, overall accuracy, kappa statistic and the F-score (Supplementary Table 1). User's accuracy is complement of the error of commission and is calculated as the correctly classified pixels within a class divided by the count of pixels that were classified as that class. Producer's accuracy is complement of the error of omission and is calculated as the correctly classified pixels within a class divided by the count of pixels that were referenced as that class in the training data. Overall accuracy indicates how effective the overall classification was and is calculated as the total correctly classified pixels divided by all of the training pixels. The accuracies range between 0% and 100%, with 100% representing total agreement between the training data and the classification.

The kappa analysis is a discrete multivariate technique used in accuracy assessment to measure the chance agreement[53,54]. Kappa values over 80% represent strong agreement between the classified images and the ground reference information[55].

The F-score provides a similar measure to overall accuracy while accounting for imbalances in the amount of training data for each class and is calculated as[56] ((user's accuracy × producer's accuracy)/(user's accuracy + producer's accuracy) × 2). The F-score ranges between 0 and 1, with 1 meaning complete agreement.

Caveats

While our datasets[57] have an overall high accuracy (Supplementary Table 1), a few caveats should be considered when using the data for other applications. Some salt patches or bare soil that were misclassified as marsh in the classified image may have been an artefact of a flooding event immediately before the image acquisition. This would result in slight underestimation of salt patch area. Shadows within built areas are sometimes classified as water, while shadows on fields are sometimes classified as the built class. The classes most often confused with one another are crop fields and other vegetation, which typically encompasses open fields and lawns. These misclassifications do not have any direct implications for salt patch estimates. The algorithm used in this work often underpredicted salt patches because the typical bright white signature of these salt patches can look different when those areas become wet, leading these areas to be classified as crop fields. Most prominent salt patches appear at elevation <1 m. Some of the areas classified as salt patches, especially at higher elevations, might be bleached siliceous minerals visible on the soil surface, leading to negligible overestimation of salt patch area.

Buffer assessment

Buffers around salt patches were used to assess the impact on farmlands surrounding the observed salt patches. Three different buffer areas were used: 50, 100 and 200 m. Round buffers on all sides of the salt patches were used with a planar distance, excluding the core patch. We estimated acreage for both salt patches and farmlands within these three buffers, which was then used to calculate the potential losses in profit.

Satellite-derived datasets for crop types

To calculate the extent of corn and soybean acreage in salt-affected and salt-adjacent lands, we used the USDA-National Agricultural Statistics Service (NASS) Cropland Data Layers[7] (spatial resolution 30 m). These are annual crop-specific data layers derived from satellite imagery. We downloaded the geospatial data layers for the three states matched with the NAIP image dates—2013 and 2017 for Delaware, 2011 and 2017 for Maryland and 2012 and 2016 for Virginia. We reprojected the files in WGS84 using ArcMap 10.8.1 making them compatible with our high-resolution data layers, before resampling those to 1 m. For corn acreage, we combined the following classes: corn, double crop winter wheat/corn, double crop oats/corn, double crop barley/corn and double crop corn/soybeans. To calculate soybean acreage, we combined the following classes: soybeans, double crop winter wheat/soybeans, double crop soybeans/oats and double crop barley/soybeans. We then used our salt patch polygons (derived from our 1 m classified images) and buffer polygons to calculate corn and soybeans acreage.

Soil EC sampling and analysis

To determine soil EC, a measure of soil salinity, we first identified areas of potential SWI using Google Earth to locate white patches on the edges of farm fields, along with farm fields regardless of the presence of visible signs of salt patches. This step was completed without consulting our geospatial datasets, to include an independent assessment of our geospatial work. We worked with the Somerset County Soil Conservation District Office (Princess Anne, Maryland) to obtain permission from landowners to sample on these properties and in the summer of 2019 we sampled 36 farm fields where we were able to obtain permission. A 3 × 3 m^2 plot was established in a salt patch on each field and a handheld Garmin GPS was used to record the location at the centre of the plot. After soil sample collection, locations of these farm sites were used to calculate the nearest distance to a salt patch in our geospatial data layer. We collected at least five soil samples from within the plot at 0–10 and 10–20 cm depths using a 2 cm push probe. Soils were homogenized by depth at the plot-level and transported

on ice back to the University of Maryland Lab for processing and EC analysis (total of 72 samples). In the laboratory, soils were mixed with deionized water in a 2:1 deionized water:soil slurry. The slurries were shaken for 1 h and allowed to settle overnight. Samples with a cloudy supernatant the next morning were centrifuged for 10 min (4,180*g*) until clear. An Orion three-electrode conductivity cell connected to a Versa Star multiparameter benchtop meter (ThermoFisher Scientific) was used to measure EC in mS cm^{-1} of the clear supernatant and the values were corrected to saturated paste equivalent measures by multiplying by the ratio of soil slurry mass to soil mass. EC was measured in triplicate on each sample.

Soil EC threshold tolerances for corn, soy and wheat are 1.7, 5.0 and 6.0 mS cm^{-1}, respectively[14]. We recorded high EC values (>5 mS cm^{-1}) hundreds of metres away from a salt patch (Supplementary Fig. 1). Thus, our three buffers of 50, 100 and 200 m from visible salt patches provide a range of estimates of at-risk farmlands.

Financial loss estimates

We used the enterprise budget tool available from the University of Maryland Extension to estimate potential profit loss for no-till corn (*Zea mays*) and soybean (*Glycine max*) grain crop production[58]. The University of Maryland enterprise budget tool calculates the profit per acre by subtracting fixed and variable costs from the gross profit (grain yields × grain price). Fixed costs include equipment costs and land rents while variable costs include seed, fertilizer and pesticide applications. We estimated profits separately for each county in Maryland, Delaware and Virginia using county-specific yields and land rental, fertilizer and harvested grain prices. We estimated potential profits on the basis of the highest annual yield during 2011–2020 for each county, based on survey data from the USDA-NASS[21]. We used these values to represent the yield that could be achieved under ideal planting and weather conditions. Thus, we attribute losses in our scenarios to soluble salts beyond crop thresholds—as opposed to climate or other factors. Due to the large interannual fluctuations in input costs and grain prices, we calculated potential profits on the basis of average per bushel profits over multiple growing seasons. Specifically, annual profits were calculated on the basis of average input and crop prices over 10 years (2011–2020). We used cash land rental prices for non-irrigated fields[21]. Fertilizer prices for nitrogen (N), phosphorus (P_2O_5) and potassium (K_2O) are based on USDA-NASS averages from 2006 to 2014[21] and numbers from Data Transmission Network/Progressive Farmer reports from 2014 to 2020 (https://www.dtnpf.com/agriculture/web/ag/home). Nitrogen prices are based on 28% urea ammonium nitrate (UAN28) prices, which is more commonly used on the Delmarva Peninsula, while P_2O_5 is based on diammonium phosphate and K_2O in potash (KCl). Harvested grain prices for the eastern shore of Maryland and Delaware are from Ag Market News published by the Maryland Department of Agriculture (https://agmarketnews.com/), while historical eastern shore Virginia grain prices are obtained from the Virginia Department of Agriculture historical grain market reports[59]. We assumed the grain prices to be September cash prices. We did not consider storage, grain marketing or crop insurance costs or returns in these budgets. We calculated potential profit loss for each county as the area affected by SWI (salt patches or salt-impacted farmlands within buffers) times the average potential per acre profits for that county.

Reporting summary

Further information on research design is available in the Nature Portfolio Reporting Summary linked to this article.

Data availability

The high-resolution dataset for salt patches and other land covers for 2011–2013 and 2016–2017 are available at https://zenodo.org/record/6685695#.Y9AiVXbMIdU.

Code availability

Sample GEE code is available along with the high-resolution dataset[57].

References

1. White, E. & Kaplan, D. Restore or retreat? Saltwater intrusion and water management in coastal wetlands. *Ecosyst. Health Sustain.* **3**, e01258 (2017).
2. Kirwan, M. L. & Gedan, K. B. Sea-level driven land conversion and the formation of ghost forests. *Nat. Clim. Change* **9**, 450–457 (2019).
3. McKenzie, T., Habel, S. & Dulai, H. Sea-level rise drives wastewater leakage to coastal waters and storm drains. *Limnol. Oceanogr. Lett.* **6**, 154–163 (2021).
4. Tully, K. et al. The invisible flood: the chemistry, ecology, and social implications of coastal saltwater intrusion. *BioScience* **69**, 368–378 (2019).
5. Tully, K. L., Weissman, D., Wyner, W. J., Miller, J. & Jordan, T. Soils in transition: saltwater intrusion alters soil chemistry in agricultural fields. *Biogeochemistry* **142**, 339–356 (2019).
6. White, E. E., Ury, E. A., Bernhardt, E. S. & Yang, X. Climate change driving widespread loss of coastal forested wetlands throughout the North American coastal plain. *Ecosystems* **25**, 812–827 (2022).
7. *C-CAP Regional Land Cover and Change* (NOAA Office for Coastal Management, accessed August 2022); www.coast.noaa.gov/htdata/raster1/landcover/bulkdownload/30m_lc/
8. DeSantis, L. R. G., Bhotika, S., Williams, K. & Putz, F. E. Sea-level rise and drought interactions accelerate forest decline on the Gulf Coast of Florida, USA. *Glob. Change Biol.* **13**, 2349–2360 (2007).
9. Sallenger, A. H., Doran, K. S. & Howd, P. A. Hotspot of accelerated sea-level rise on the Atlantic coast of North America. *Nat. Clim. Change* **2**, 884–888 (2012).
10. Fagherazzi, S. et al. Sea level rise and the dynamics of the marsh–upland boundary. *Front. Environ. Sci.* **7**, 25 (2019).
11. Sweet, W. V. et al. *Global and Regional Sea Level Rise Scenarios for the United States: Updated Mean Projections and Extreme Water Level Probabilities Along U.S. Coastlines* (NOAA, 2022); https://oceanservice.noaa.gov/hazards/sealevelrise/noaa-nos-techrpt01-global-regional-SLR-scenarios-US.pdf
12. Ury, E. A., Wright, J. P., Ardón, M. & Bernhardt, E. S. Saltwater intrusion in context: soil factors regulate impacts of salinity on soil carbon cycling. *Biogeochemistry* **157**, 215–226 (2022).
13. Maas, E. V. & Grattan, S. R. in *Crop Yields as Affected by Salinity* (eds Skaggs, R. W. & van Schilfgaarde, J.) 55–108 (ASA, 1999).
14. Tanji, K. K. & Kielen, N. C. *Agricultural Drainage Water Management in Arid and Semi-arid Areas. Annex 1. Crop Salt Tolerance Data* (FAO, 2002).
15. Zörb, C., Geilfus, C.-M. & Dietz, K.-J. Salinity and crop yield. *Plant Biol. J.* **21**, 31–38 (2019).
16. de la Reguera, E., Veatch, J., Gedan, K. & Tully, K. L. The effects of saltwater intrusion on germination success of standard and alternative crops. *Environ. Exp. Bot.* **180**, 104254 (2020).
17. Titus, J. G. et al. State and local governments plan for development of most land vulnerable to rising sea level along the US Atlantic coast. *Environ. Res. Lett.* **4**, 044008 (2009).
18. *Cropscape—Cropland Data Layer* (USDA-NASS, accessed 24 August 2022); https://nassgeodata.gmu.edu/CropScape/
19. Ullah, A., Bano, A. & Khan, N. Climate change and salinity effects on crops and chemical communication between plants and plant growth-promoting microorganisms under stress. *Front. Sustain. Food Syst.* **5**, 618092 (2021).
20. Devkota, K. P., Devkota, M., Rezaei, M. & Oosterbaan, R. Managing salinity for sustainable agricultural production in salt-affected soils of irrigated drylands. *Agric. Syst.* **198**, 103390 (2022).
21. *National Agricultural Statistics Service Surveys* (NASS, accessed 24 August 2022); https://www.nass.usda.gov/Surveys/Guide_to_NASS_Surveys/index.php

22. Schieder, N. W., Walters, D. C. & Kirwan, M. L. Massive upland to wetland conversion compensated for historical marsh loss in chesapeake Bay, USA. *Estuaries Coasts* **41**, 940–951 (2018).
23. Schroeder, C. S., Kulick, N. K. & Farrer, E. C. Saltwater intrusion indirectly intensifies *Phragmites australis* invasion via alteration of soil microbes. *Sci. Rep.* **12**, 16582 (2022).
24. Epanchin-Niell, R., Kousky, C., Thompson, A. & Walls, M. Threatened protection: sea level rise and coastal protected lands of the eastern United States. *Ocean Coast. Manag.* **137**, 118–130 (2017).
25. Gedan, K. B., Epanchin-Niell, R. & Qi, M. Rapid land cover change in a submerging coastal county. *Wetlands* **40**, 1717–1728 (2020).
26. Gardner, L. R. et al. Disturbance effects of Hurricane Hugo on a pristine coastal landscape: North Inlet, South Carolina, USA. *Netherl. J. Sea Res.* **30**, 249–263 (1992).
27. Allen, J. A., Conner, W. H., Goyer, R. A., Chambers, J. L., & Krauss, K. W. Freshwater forested wetlands and global climate change. In *Vulnerability of Coastal Wetlands in the Southeastern United States: Climate Change Research Results 1992–1997* (eds Guntenspergen, G. R. & Vairin, B. A.) 33–44 (U.S. Geological Survey, 1998).
28. Domagalski, J. L. et al. *Comparative Water-Quality Assessment of the Hai He River Basin in the People's Republic of China and Three Similar Basins in the United States* (USGS, 2001).
29. Karegar, M. A., Dixon, T. H., Malservisi, R., Kusche, J. & Engelhart, S. E. Nuisance flooding and relative sea-level rise: the importance of present-day land motion. *Sci. Rep.* **7**, 11197 (2017).
30. Steppuhn, H., van Genuchten, M. T. & Grieve, C. M. Root-zone salinity. *Crop Sci.* **45**, 221–232 (2005).
31. Bhattachan, A. et al. Evaluating the effects of land-use change and future climate change on vulnerability of coastal landscapes to saltwater intrusion. *Elementa* **6**, 62 (2018).
32. Goebel, M., Pidlisecky, A. & Knight, R. Resistivity imaging reveals complex pattern of saltwater intrusion along Monterey coast. *J. Hydrol.* **551**, 746–755 (2017).
33. Da Lio, C., Carol, E., Kruse, E., Teatini, P. & Tosi, L. Saltwater contamination in the managed low-lying farmland of the Venice coast, Italy: an assessment of vulnerability. *Sci. Total Environ.* **533**, 356–369 (2015).
34. Genua-Olmedo, A., Alcaraz, C., Caiola, N. & Ibáñez, C. Sea level rise impacts on rice production: the Ebro Delta as an example. *Sci. Total Environ.* **571**, 1200–1210 (2016).
35. Michael, H. A., Russoniello, C. J. & Byron, L. A. Global assessment of vulnerability to sea-level rise in topography-limited and recharge-limited coastal groundwater systems. *Water Resour. Res.* **49**, 2228–2240 (2013).
36. Nordio, G. & Fagherazzi, S. Groundwater, soil moisture, light and weather data collected in a coastal forest bordering a salt marsh in the Delmarva Peninsula (VA). *Data Brief.* **45**, 108584 (2022).
37. Nordio, G. et al. Frequent storm surges affect the groundwater of coastal ecosystems. *Geophys. Res. Lett.* **50**, e2022GL100191 (2023).
38. *Global Map of Salt-affected Soils (GSASmap)* (FAO, accessed 24 August 2022); https://www.fao.org/soils-portal/data-hub/soil-maps-and-databases/global-map-of-salt-affected-soils/en/
39. Guimond, J. A. & Michael, H. A. Effects of marsh migration on flooding, saltwater intrusion, and crop yield in coastal agricultural land subject to storm surge inundation. *Water Res.* **57**, e2020WR028326 (2021).
40. Sternberg, L. S. L., Teh, S. Y., Ewe, S. M., Miralles-Wilhelm, F. & DeAngelis, D. L. Competition between hardwood hammocks and mangroves. *Ecosystems* **10**, 648–660 (2007).
41. Wendelberger, K. S. & Richards, J. H. Halophytes can salinize soil when competing with glycophytes, intensifying effects of sea level rise in coastal communities. *Oecologia* **184**, 729–737 (2017).
42. Poulter, B., Christensen, N. L. & Song, Q. S. Tolerance of *Pinus taeda* and *Pinus serotina* to low salinity and flooding: implications for equilibrium vegetation dynamics. *J. Veg. Sci.* **19**, 15–122 (2008).
43. *Google Earth Engine Guides. Eigen Analysis* (Google, 2021); https://developers.google.com/earth-engine/guides/arrays_eigen_analysis
44. McFeeters, S. K. The use of the normalized difference water index (NDWI) in the delineation of open water features. *Int. J. Remote Sens.* **17**, 1425–1432 (1996).
45. Townshend, J. R. G., Goff, T. E. & Tucker, C. J. Multitemporal dimensionality of images of normalized difference vegetation index at continental scales. *IEEE Trans. Geosci. Remote Sens.* **23**, 888–895 (1985).
46. Maxwell, A. E., Warner, T. A., Vanderbilt, B. C. & Ramezan, C. A. Land cover classification and feature extraction from national agriculture imagery program (NAIP) orthoimagery: a review. *Photogramm. Eng. Remote Sens.* **83**, 737–747 (2017).
47. Karl Pearson, F. R. S. L. III On lines and planes of closest fit to systems of points in space. *Philos. Mag.* **2**, 559–572 (1901).
48. Dharani, M. & Sreenivasulu, G. Land use and land cover change detection by using principal component analysis and morphological operations in remote sensing applications. *Int. J. Comput. Appl.* **43**, 462–471 (2021).
49. *Google Earth Engine Guides. Eigen Analysis* (Google, 2023); https://developers.google.com/earth-engine/guides/arrays_eigen_analysis
50. Xue, J. & Su, B. Significant remote sensing vegetation indices: a review of developments and applications. *J. Sens.* **2017**, 1353691 (2017).
51. *Google Earth Engine Guides. Convolutions* (Google, 2022); https://developers.google.com/earth-engine/guides/image_convolutions
52. Breiman, L. Random Forests. *Mach. Learn.* **45**, 5–32 (2001).
53. Congalton, R. G., Oderwald, R. G. & Mead, R. A. Assessing landsat classification accuracy using discrete multivariate analysis statistical. *Tech. Photogramm Eng. Remote Sens.* **49**, 1671–1678 (1983).
54. Congalton, R. G. A review of assessing the accuracy of classifications of remotely sensed data. *Remote Sens. Environ.* **37**, 35–46 (1991).
55. Landis, J. R. & Koch, G. G. The measurement of observer agreement for categorical data. *Biometrics* **33**, 159–174 (1977).
56. Maxwell, A. E. & Warner, T. A. Thematic classification accuracy assessment with inherently uncertain boundaries: an argument for center-weighted accuracy assessment metrics. *Remote Sens* **12**, 1905 (2020).
57. Mondal, P. et al. High-resolution remotely sensed datasets for saltwater intrusion across the Delmarva Peninsula [data set]. *Zenodo* https://doi.org/10.5281/zenodo.6685695 (2022).
58. Dill, S., Beale, B., Johnson, D., Lewis, J. & Rhodes, J. *2022 Field Crop Budgets* (Univ. Maryland Extension, 2022); https://extension.umd.edu/resource/field-crop-budgets
59. *Virginia Grain Historical Prices* (Virginia Department of Agriculture and Consumer Service, 2021); https://www.vdacs.virginia.gov/markets-and-finance-market-news-grain-stats.shtml

Acknowledgements

This publication was made possible by the National Science Foundation EPSCoR grant no. 1757353 and the State of Delaware that supported P.M. and V.Y. This work was also supported by the National Aeronautics and Space Administration EPSCoR grant DE-80NSSC20M0220 awarded to P.M., the Delaware Space Grant College and Fellowship Program (NASA grant 80NSSC20M0045) that supported M.W. and the USDA-National Institute for Food and Agriculture (grant 12451226) awarded to J.M., R.E.-N., K.G. and K.T. We acknowledge the support provided to P.M., M.W., J.M., R.E.-N., K.G. and K.T. by the US Environmental Protection Agency (Assistance Agreement no. CB96358101), USDA Natural Resources Conservation Service (Assistance Agreement no. NR193A750007C005) and the

National Fish and Wildlife Foundation's Chesapeake Bay Stewardship Fund (grant 0603.20.071142), as well as the State of Maryland and Harry R. Hughes Center for Agro-Ecology. The funders had no role in study design, data collection and analysis, decision to publish or preparation of the manuscript.

Author contributions

P.M. developed the overall study concept and design. K.T. conceived and designed the electrical conductivity analysis. R.E.-N. contributed in certain aspects of the study design. M.W. and P.M. processed, developed and analysed the geospatial data. K.T. and E.N. collected and analysed soil samples. J.M., V.Y. and E.N. contributed to further data analysis. P.M. prepared the first draft of the paper. M.W., K.G., R.E.-N. and K.T. contributed to the writing.

Competing interests

The authors declare no competing interests.

Additional information

Supplementary information The online version contains supplementary material available at https://doi.org/10.1038/s41893-023-01186-6.

Correspondence and requests for materials should be addressed to Pinki Mondal.

Peer review information *Nature Sustainability* thanks Cristoph-Martin Geilfus, Elliott White and the other, anonymous, reviewer(s) for their contribution to the peer review of this work.

nature portfolio

Corresponding author(s): Pinki Mondal

Last updated by author(s): Jun 23, 2023

Reporting Summary

Nature Portfolio wishes to improve the reproducibility of the work that we publish. This form provides structure for consistency and transparency in reporting. For further information on Nature Portfolio policies, see our Editorial Policies and the Editorial Policy Checklist.

Statistics

For all statistical analyses, confirm that the following items are present in the figure legend, table legend, main text, or Methods section.

n/a	Confirmed
☐	☒ The exact sample size (*n*) for each experimental group/condition, given as a discrete number and unit of measurement
☐	☒ A statement on whether measurements were taken from distinct samples or whether the same sample was measured repeatedly
☒	☐ The statistical test(s) used AND whether they are one- or two-sided *Only common tests should be described solely by name; describe more complex techniques in the Methods section.*
☒	☐ A description of all covariates tested
☒	☐ A description of any assumptions or corrections, such as tests of normality and adjustment for multiple comparisons
☒	☐ A full description of the statistical parameters including central tendency (e.g. means) or other basic estimates (e.g. regression coefficient) AND variation (e.g. standard deviation) or associated estimates of uncertainty (e.g. confidence intervals)
☒	☐ For null hypothesis testing, the test statistic (e.g. *F*, *t*, *r*) with confidence intervals, effect sizes, degrees of freedom and *P* value noted *Give P values as exact values whenever suitable.*
☒	☐ For Bayesian analysis, information on the choice of priors and Markov chain Monte Carlo settings
☒	☐ For hierarchical and complex designs, identification of the appropriate level for tests and full reporting of outcomes
☒	☐ Estimates of effect sizes (e.g. Cohen's *d*, Pearson's *r*), indicating how they were calculated

Our web collection on statistics for biologists contains articles on many of the points above.

Software and code

Policy information about availability of computer code

Data collection	Remotely sensed data (aerial data from the National Agriculture Imagery Program, and satellite data from Landsat) were analyzed using the cloud computing platform Google Earth Engine (GEE). All input images are freely available on GEE. Satellite-derived datasets for crop types are from the USDA-NASS Cropland Data Layers.
Data analysis	We used a cloud computing platform, Google Earth Engine (GEE), for running the Random Forest algorithm from the Statistical Machine Intelligence and Learning Engine (SMILE). Post-processing of classified images were performed using ArcGIS Pro version 3.0.3. Figures were created using ArcMap 10.8.1, and Microsoft PowerPoint 2016.

For manuscripts utilizing custom algorithms or software that are central to the research but not yet described in published literature, software must be made available to editors and reviewers. We strongly encourage code deposition in a community repository (e.g. GitHub). See the Nature Portfolio guidelines for submitting code & software for further information.

Data

Policy information about availability of data

All manuscripts must include a data availability statement. This statement should provide the following information, where applicable:

- Accession codes, unique identifiers, or web links for publicly available datasets
- A description of any restrictions on data availability
- For clinical datasets or third party data, please ensure that the statement adheres to our policy

The high-resolution dataset for salt patches and other land covers for 2011-2013 and 2016-2017 are available at https://zenodo.org/record/6685695#.Y9AiVXbMIdU (DOI: 10.5281/zenodo.6685695).

Human research participants

Policy information about studies involving human research participants and Sex and Gender in Research.

Reporting on sex and gender	N/A
Population characteristics	N/A
Recruitment	N/A
Ethics oversight	N/A

Note that full information on the approval of the study protocol must also be provided in the manuscript.

Field-specific reporting

Please select the one below that is the best fit for your research. If you are not sure, read the appropriate sections before making your selection.

☐ Life sciences ☐ Behavioural & social sciences ☒ Ecological, evolutionary & environmental sciences

For a reference copy of the document with all sections, see nature.com/documents/nr-reporting-summary-flat.pdf

Ecological, evolutionary & environmental sciences study design

All studies must disclose on these points even when the disclosure is negative.

Study description	This study involves analyzing freely available aerial and satellite images (analyzed using Google Earth Engine) to identify salt patch signatures on bare soil. Soil samples were collected for Electrical Conductivity (EC) analysis to compare with remotely sensed data. Freely available crop census data (source: USDA) were used to calculate potential loss in profit.
Research sample	For the EC analysis, we sampled 36 farm fields in summer 2019. A total of 72 samples were analyzed (to represent 2 depths: 0-10 cm and 10-20 cm).
Sampling strategy	We worked with the Somerset County Soil Conservation District Office (Princess Anne, MD) to obtain permission from landowners to sample on 36 farms. To select these firms, we identified areas of potential saltwater intrusion using Google Earth to locate white patches on the edges of farm fields, along with farm fields regardless of the presence of visible signs of salt patches. A 3 x 3 m plot was established in a salt patch on each field, and a handheld Garmin GPS was used to record the location at the center of the plot.
Data collection	We collected at least 5 soil samples from within the plot at 0-10 cm and 10-20 cm depths using a 2-cm push probe. Soils were homogenized by depth at the plot-level and transported on ice back to the University of Maryland Lab for processing and EC analysis (total of 72 samples). Dr. Kate Tully and Elizabeth Nguyen were in charge of this analysis.
Timing and spatial scale	Soil samples were collected from 36 farms in the summer of 2019 during a 3-month sampling campaign. Summer months were selected to avoid the end of growing season when the crops are fully grown.
Data exclusions	For this study we only used soil samples collected on a farmland, and excluded soil samples collected from a forest, since the focus of our study is on farmlands.
Reproducibility	Each soil sample was measured for EC in triplicate to ensure accuracy. When replicates were more than 10% different from each other, the probe was re-calibrated. The EC probe was calibrated every day before measuring soil EC.
Randomization	Five soil cores were collected at random in the 3 x 3 meter plot, but homogenized at the plot-level.
Blinding	N/A

Did the study involve field work? ☒ Yes ☐ No

Field work, collection and transport

Field conditions	Soils were collected from private lands on the Lower Eastern Shore of Maryland. Annual precipitation is 1085 mm per year. Sea level rise rates in the region have increased from ~1–3 mm per year in the 1930s to ~4–10 mm year in 2011.
Location	Soils were collected from private lands on the Lower Eastern Shore of Maryland.
Access & import/export	Soils were collected with landowner permission with help of the Somerset County Soil Conservation District Office.
Disturbance	After soils were collected, holes were backfilled.

Reporting for specific materials, systems and methods

We require information from authors about some types of materials, experimental systems and methods used in many studies. Here, indicate whether each material, system or method listed is relevant to your study. If you are not sure if a list item applies to your research, read the appropriate section before selecting a response.

Materials & experimental systems

n/a	Involved in the study
☒	☐ Antibodies
☒	☐ Eukaryotic cell lines
☒	☐ Palaeontology and archaeology
☒	☐ Animals and other organisms
☒	☐ Clinical data
☒	☐ Dual use research of concern

Methods

n/a	Involved in the study
☒	☐ ChIP-seq
☒	☐ Flow cytometry
☒	☐ MRI-based neuroimaging